Line-Constrained-Based Explicit Model Predictive Current Control for IPMSMs Drives

Han Wang, Jianyong Su, *Member, IEEE*, and Guijie Yang, *Member, IEEE*

***Abstract*—This article proposes an improved line-constrained explicit model predictive control (EMPC) method for interior permanent magnet synchronous motors by utilizing the constraint processing capability of EMPC. Despite the substantial advantages that EMPC provides for motor drives, its memory occupancy and complex weight factor calculation make it limited in tackling only small-scale issues. To address these challenges, the improved method incorporates a constraint variable that converts the area constraints of the conventional EMPC strategy into line constraints. The findings demonstrate that the line-constrained EMPC minimizes the number of piecewise affine regions to fewer than ten, which is substantially fewer than those of the conventional method, hence significantly decreasing the algorithm's memory occupancy rate. Moreover, only one weight factor in the cost function exists in the proposed approach, which solves the weight factor calculation problem inherent in the EMPC method. This method's superiority is demonstrated through simulations and experiments.**

***Index Terms*—Interior permanent magnet synchronous motors (IPMSMs) drives, line-constrained explicit model predictive control (EMPC), memory occupancy, piecewise affine (PWA) regions, weight factors calculation.**

I. Introduction

DUE to their high power density and high load capacity, interior permanent magnet synchronous motors (IPMSMs) are widely used in the field of electric vehicles [1]. The traditional field-oriented control (FOC) method employs proportional-integral (PI) controllers, but PI controllers are single-input single-output, making system overall optimization and constraints application challenging to achieve [2]. Moreover, the issue of PI parameter tuning has not been satisfactorily resolved. With the continual increase of control performance criteria, PI controllers cannot match the requirements; thus, several other algorithms are proposed, among which model predictive control (MPC) is the most effective.

MPC is based on an explicit and identifiable model of the controlled system, which is used to precalculate the behavior of the plant and choose an optimal value of the control variables [3]. MPC is classified as finite control set (FCS) and continuous control set (CCS). FCS-MPC has been widely adopted because of its flexible constraint processing capacity, no need for an extra modulator and faster dynamic response than FOC [4], [5]. However, there will be significant ripples in the current and the torque as its control set is based on discrete voltage vectors [6]. CCS-MPC converts the control objective into a quadratic programming (QP) problem [7], [8], [9] and have demonstrated its effectiveness in reducing current and torque ripples. Due to the extensive calculations required for online optimization, CCS-MPC cannot be implemented on low-cost platforms [10].

Explicit model predictive control (EMPC) converts a portion of the CCS-MPCs online optimization to offline computing via a PWA fashion [11], [12]. Due to its powerful constraint-handling capability, EMPC is preferable for motor-drive systems. Nevertheless, EMPC is only suited for small-scale systems due to the polynomial memory that PWA regions occupy and logarithmic search time [13], [14], [15]. In addition, the intricacy of calculating weight factors also limits the EMPC application.

The memory occupancy of the PWA regions is determined by the model's dimensions, constraints, and the prediction horizon's length. For the model dimension, the traditional method added the coupling terms to the prediction model as measured disturbances, therefore increasing the system dimension. For example, Bolognani et al. [3] presented seven-dimensional (7-D) state variables to implement $i_d = 0$ control of surface-mounted permanent magnet synchronous motors, whereas Mynar et al. [2] introduced 9 to implement flux-weakening control of IPMSMs. The measured disturbances increase the algorithm's parameter sensitivity and memory occupancy. The observer-combination strategy is an appealing solution for this issue [16], [17]. In [18], a deadbeat controller based on an extended state observer (ESO) utilizing an ultralocal model is suggested, which reduces the motor model's reliance and simplifies the prediction model. As for the prediction horizon's length, Bolognani et al. [3] determined, based on the sampling delay, that there is a minimum value to ensure that all state variables are updated. Nevertheless, it should be noted that the constraints have the greatest impact on memory occupancy rather than the model's dimensions or prediction horizon's length.

The number and form of EMPC constraints have a direct impact on the PWA regions [19]. In the traditional method, the constraints processing capability of EMPC is employed to handle overcurrent and overvoltage protection, termed area constraints in this article. However, the area constraints result in a huge number of PWA regions, which will significantly raise the memory occupancy and logarithmic search time of EMPC, restricting its implementation on low-cost platforms.

Manuscript received 15 December 2022; revised 21 March 2023; accepted 3 May 2023. Date of publication 10 May 2023; date of current version 21 June 2023. Recommended for publication by Associate Editor Zhenbin Zhang. *(Corresponding author: Han Wang.)*

The authors are with the Department of Electrical Engineering, Harbin Institute of Technology, Harbin 150001, China (e-mail: 20b906035@stu.hit.edu.cn; sujianyong@hit.edu.cn; yangguijie@hit.edu.cn).

Color versions of one or more figures in this article are available at https://doi.org/10.1109/TPEL.2023.3274839.

Digital Object Identifier 10.1109/TPEL.2023.3274839

Another issue with EMPC is the complex weight factor calculation. It is often necessary to employ weight factors due to the inability to unify various objectives [20]. Caseiro et al. [21] and Machado et al. [22] introduced artificial neural networks (ANNs) to online calculate the weight factors, but this would increase the algorithm's computing burden. Utilizing ANNs offline in [23] to compute the weight factors of torque and flux linkage increases the algorithm's memory use, which is not anticipated by EMPC.

The main contribution of this article is to propose a line-constrained EMPC method that reduces memory occupancy and solves the weight factor calculation problem, allowing the algorithm to run on low-cost platforms. The improved method incorporates a constraint variable into the prediction model, which converts the area constraints of the conventional algorithm into line constraints and employs the constraint processing capability of EMPC to track the d-axis current reference. In order to minimize the system dimension, the ultralocal model with ESO is used to construct the EMPC prediction model. The results reveal that the line-constrained EMPC decreases the number of PWA regions to less than 10, which is much less than the conventional method, hence reduces the algorithm's memory occupancy. The proposed algorithm's cost function has only one weight factor, which has no effect on the system's performance, so there is no need to consider weight factor calculation. The proposed method has been implemented on Infineon's XMC4500 platform, and the PWA space has been created using the multiparametric toolbox [24]. Experiments and simulations demonstrate the superiority of the proposed method.

The rest of this article is organized as follows. Section II deduces the mathematical model. Section III proposes a line-constrained EMPC method, and the robustness of the weight factor is analyzed. In Sections IV and V, the proposed algorithm's superiority is demonstrated through simulations and experiments. Finally, Section VI concludes this article.

II. Mathematical Model

A. PMSM Model

The electrical components of the IPMSM model can be expanded in a rotating frame to achieve decoupling. The following electrical components can be deduced:

$$\begin{cases} \frac{di_d}{dt} = \frac{1}{L_d}(u_d - Ri_d + \omega L_q i_q) \\ \frac{di_q}{dt} = \frac{1}{L_q}(u_q - Ri_q - L_d\omega i_d - \omega\lambda_r) \end{cases} \tag{1}$$

where R is the stator phase resistance; i_d and i_d are the stator dq-axis currents; u_d and u_q denote the stator voltage vectors; λ_r is the rotor flux linkage; ω represents the electrical rotor speed; and L_d and L_q are the dq-axis inductances.

Using Euler discretization, the following discrete model can be obtained:

$$\begin{cases} i_d(k+1) = i_d(k) + \frac{T}{L_d}(u_d(k) - Ri_d(k) + \omega L_q i_q(k)) \\ i_q(k+1) = i_q(k) + \frac{T}{L_q}(u_q(k) - Ri_q(k) - L_d\omega i_d(k) - \omega\lambda_r) \end{cases} \tag{2}$$

where T is the sampling time. In this article, the motor's mathematical model is reconstructed using the ultralocal model with ESO, as presented in [18], in order to minimize the model's dimension and reduce sensitivity to the motor's parameters. The reconstructed motor model is given as follows:

$$\begin{cases} i_d(k+1) = \alpha_d u_d(k) + F_d(k) \\ i_q(k+1) = \alpha_q u_q(k) + F_q(k) \end{cases} \tag{3}$$

where $\alpha_d = \frac{T}{L_d}$, $\alpha_q = \frac{T}{L_q}$, $F_d(k) = \frac{T}{L_d}(-Ri_d(k) + \omega L_q i_q(k))$, and $F_q(k) = \frac{T}{L_d}(-Ri_q(k) - L_d\omega i_d(k) - \omega\lambda_r)$.

The ESO is designed as follows:

$$\begin{cases} \dot{\hat{x}}_{ob} = (A_{ob} - LC)\hat{x} + B_{ob}u + Ly \\ \hat{y} = C\hat{x} \end{cases} \tag{4}$$

where L is a parameter matrix that changes the observer's closed-loop poles. The observer's state and input variables are chosen as follows:

$$\begin{aligned} \hat{x}_{ob} &= \begin{bmatrix} \hat{i}_d(k) & \hat{i}_q(k) & \hat{F}_d(k) & \hat{F}_q(k) \end{bmatrix}^T \\ u &= \begin{bmatrix} u_d(k) & u_q(k) \end{bmatrix}^T. \end{aligned} \tag{5}$$

The observer state equation matrix is given as follows

$$\begin{aligned} A_{ob} &= \begin{bmatrix} 1 & 0 & 1 & 0 \\ 0 & 1 & 0 & 1 \\ 0 & 0 & 1 & 0 \\ 0 & 0 & 0 & 1 \end{bmatrix}, \quad B_{ob} = \begin{bmatrix} \alpha_{\mathrm{d}} & 0 \\ 0 & \alpha_{\mathrm{q}} \\ 0 & 0 \\ 0 & 0 \end{bmatrix} \\ C &= \begin{bmatrix} 1 & 0 & 0 & 0 \\ 0 & 1 & 0 & 0 \end{bmatrix}. \end{aligned} \tag{6}$$

Since the observation loop's closed-loop poles are the eigenvalues of $(A_{ob} - LC)$, L should be designed so that the closed-loop poles converge inside the unit circle.

B. EMPC Algorithm

The discrete mathematical model of the system is given as follows:

$$\begin{aligned} x(k+1) &= Ax(k) + Bu(k) \\ y(k) &= Cx(k) + Du(k). \end{aligned} \tag{7}$$

Assuming that $D = 0$, the notion of EMPC is based on multiparametric QP [25]. The control goal is described as a cost function that solves constrained multiparametric optimization problems

$$\begin{aligned} &J(k) = x(k+N_p)^T P x(k+N_p) \\ &+ \sum_{j=0}^{N_p-1} \left[x(k+j)^T Q x(k+j) + u(k+j)^T R_u u(k+j) \right] \\ &\text{s.t.} \\ &\forall j \in [0, N_p - 1] \quad x(k+j+1) = Ax(k+j) + Bu(k+j) \\ &\forall j \in [1, N_p] \qquad x(k+j) \in \chi \subset R^n \\ &\forall j \in [1, N_p] \qquad u(k+j) \in \mu \subset R^m \end{aligned} \tag{8}$$

where P and Q are the positive semidefinite weighting vectors, the positive definite matrix R_u penalizes control action, N_p is the prediction horizon, and χ and μ represent the state and input constraints, respectively. By iterating, the system state at

step $k+j$ is converted into the following equation:

$$x(k+j) = A^j x(k) + \sum_{t=0}^{j-1} A^t B u(k+j-1-t). \quad (9)$$

Using iterative (9), the cost function (8) can be transformed into a QP optimization problem with constraints

$$J(k) = \frac{1}{2}x(k)^T Y x(k) + \min_U \left[\frac{1}{2}U^T H U + x(k)^T F U\right]$$
$$\text{s.t.} GU \le W + Ex(k) \quad (10)$$

where $U = [u(k)^T, \ldots, u(k+N_u-1)^T]^T \in R^{m \cdot N_u}$, N_u is the control horizon and Y, H, F, G, W, E, and Y can be obtained by iterative Q, R_u, and constraints expressed in (8).

C. EMPC Constraints Solution

Constraints in EMPC are classified as active constraints, which refer to the limiting of state and input that have been affected, and inactive constraints

$$GU \le W + Ex(k) \Rightarrow \begin{cases} G_{ac}U = W_{ac} + E_{ac}x(k) \\ G_{ia}U < W_{ia} + E_{ia}x(k). \end{cases} \quad (11)$$

Combinations of constraints can result in the formation of affine regions, and the collections of affine spaces are referred to as PWA regions. By judging which active constraints are met by the feedback state, the area to which the state belongs can be determined, and the region's optimal solution can be obtained using the Karush–Kuhn–Tucker conditions

$$U = -H^{-1} \cdot \left(Fx(k) + G_{ac}^T \lambda\right)$$
$$\lambda = M_{ac}x(k) + m_{ac} \quad (12)$$

where

$$\begin{cases} M_{ac} = -\left(G_{ac}H^{-1}G_{ac}^T\right)^{-1} \cdot \left(E_{ac} + G_{ac}H^{-1}F\right) \\ m_{ac} = -\left(G_{ac}H^{-1}G_{ac}^T\right)^{-1} \cdot W_{ac}. \end{cases}$$

Through (12), EMPC converts the online optimization issue to offline computing, enabling EMPC to have a strong capacity to cope with constraints while minimizing computation.

III. IPMSM EMPC Algorithm

A. Model Construction of Line-Constrained EMPC

For a motor with strong convex polarity, the conventional $i_d = 0$ control cannot match the system's criteria for the minimal loss under load. Maximum torque per ampere (MTPA) control becomes an essential option. The traditional approach for implementing MTPA with an EMPC controller entails incorporating the dq-axis current references into the prediction model and then determining the optimal solution through the cost function, as seen in Fig. 1(a). However, the traditional approach cannot be implemented on a low-cost platform because of the excessive number of PWA regions formed because too many PWA regions will result in excessive memory use. This article proposes a line-constrained EMPC method to minimize the number of regions.

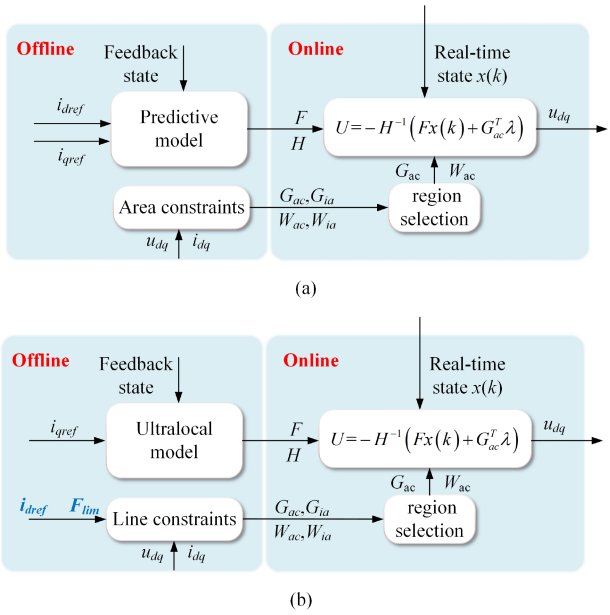

Fig. 1. Traditional and proposed MTPA implementation diagrams based on the EMPC controller. (a) is the traditional area-constrained EMPC approach. (b) is the proposed line-constrained EMPC approach.

Line-constrained EMPC reconstructs the form and scope of the constraints, and its implementation needs the introduction of a constraint variable F_{lim}, which is utilized in the MTPA approach to track the d-axis current reference. The state variables of the prediction model, according to (3) and (7), are chosen as follows:

$$x = [i_d(k) i_q(k) F_d(k) F_q(k) i_{q\text{ref}}(k) F_{\text{lim}}(k)]^T$$
$$u = [u_d(k) u_q(k)]^T \quad (13)$$

where $i_{q\text{ref}}$ is the q-axis current reference introduced into the prediction model. Assume that F_d and F_q remain constant over a short sampling time and that their differential can be regarded as zero, the system's prediction model is given as follows:

$$A = \begin{bmatrix} 1 & 0 & 1 & 0 & 0 & 0 \\ 0 & 1 & 0 & 1 & 0 & 0 \\ 0 & 0 & 1 & 0 & 0 & 0 \\ 0 & 0 & 0 & 1 & 0 & 0 \\ 0 & 0 & 0 & 0 & 1 & 0 \\ 0 & 0 & 0 & 0 & 0 & 1 \end{bmatrix}, \quad B = \begin{bmatrix} \alpha_{\text{d}} & 0 \\ 0 & \alpha_{\text{q}} \\ 0 & 0 \\ 0 & 0 \\ 0 & 0 \\ 0 & 0 \end{bmatrix}$$
$$C = \begin{bmatrix} 1 & 0 & 0 & 0 & 0 & 0 \\ 0 & 1 & 0 & 0 & 0 & 0 \end{bmatrix}. \quad (14)$$

Fig. 1(b) illustrates the improved algorithm's block diagram. Compared with Fig. 1(a), the improved algorithm assigns $i_{d\text{ref}}$ to F_{lim} and transforms the tracking of $i_{d\text{ref}}$ from cost function (8) to constraint condition (11) according to formulae (8), (11), and (12). The modification of the constraints changes the PWA active region and the calculation of G_{ac}, hence altering the result of (12).

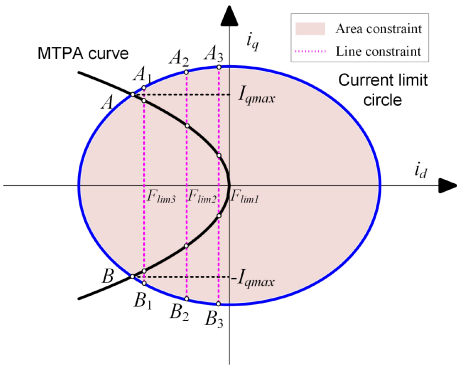

Fig. 2. Comparative diagram between line and area constraints.

B. Line Constraints Expression

Fig. 2 depicts the concept of the line-constrained EMPC. The currents in the conventional algorithm are restricted to the interior of the current limit circle, which is depicted in Fig. 2, as the area constraints. However, the d-axis current in line-constrained EMPC is bound by F_{lim} at the ith instant, where $i = 1, 2, \ldots$. The current vector is constrained to the line segment from A_i to B_i; hence, the area constraints are turned into the line constraints. Since an area contains far more data than a line segment, the number of PWA regions will be drastically reduced. In addition, state variable constraints need only limit i_q between $-I_{q\text{max}}$ and $I_{q\text{max}}$. The traditional area constraints of the current can be stated using the following formula, according to Liu et al. [26]

$$G \cdot I_{dq} \le I_{\text{max}} \cdot E \tag{15}$$

where I_{max} is the maximum current allowed

$$I_{dq} = \begin{bmatrix} i_d(k) \\ i_q(k) \end{bmatrix} \quad E = \begin{bmatrix} 1 & 1 & 1 & 1 & 1 & 1 \end{bmatrix}^T$$

$$G = \begin{bmatrix} -1 & -1 & 0 & 0 & 1 & 1 \\ \frac{-1}{\sqrt{3}} & \frac{1}{\sqrt{3}} & \frac{2}{\sqrt{3}} & \frac{-2}{\sqrt{3}} & \frac{-1}{\sqrt{3}} & \frac{1}{\sqrt{3}} \end{bmatrix}^T.$$

The formula for the current line constraints proposed in this study is given as follows:

$$\begin{cases} i_d = F_{\text{lim}} \\ -I_{q\text{max}} \le i_q \le I_{q\text{max}} \end{cases} \tag{16}$$

where $I_{q\text{max}}$ is the maximum q-axis current allowed.

The PWA regions in Fig. 3 are expanded on a 3-D space with axes i_d, i_q, and F_{lim}. It should be noted that the complexity of PWA regions increases exponentially with the number of constraints. Fig. 3 utilizes an affine law that is less complex to illustrate the comparison of PWA regions in a more comprehensible manner. Specifically, the affine law adopted in Fig. 3(a) is given as follows:

$$\begin{cases} -20\ A \le i_d \le 20\ A \\ -20\ A \le i_q \le 20\ A. \end{cases} \tag{17}$$

The affine law adopted in Fig. 3(b) is given as follows:

$$\begin{cases} -20\ A \le i_d \le 20\ A \\ -20\ A \le i_q \le 20\ A \\ i_d = F_{\text{lim}}\ . \end{cases} \tag{18}$$

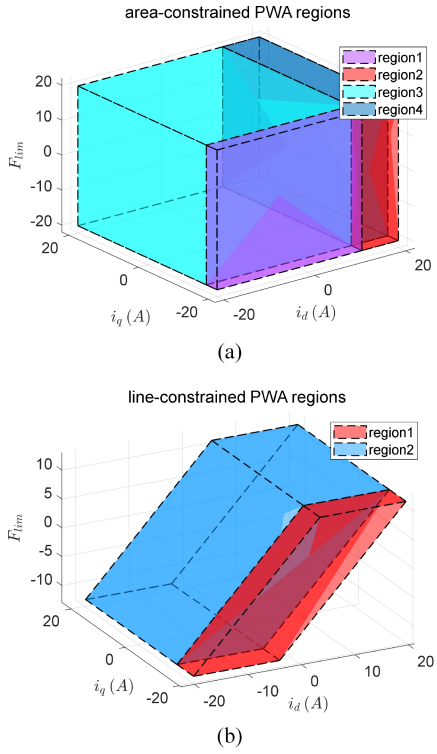

Fig. 3. PWA regions of the 3-D controller subject to (a) area constraints and (b) line constraints.

The figure demonstrates that the number of PWA regions of an EMPC controller with line constraints is reduced from four to two, and the domain of state variables is likewise much reduced. In the context of EMPC, a reduction in the domain corresponds to lower data storage requirements, while a decrease in the number of regions leads to a reduction in the number of algorithm iterations required. Consequently, the line-constrained EMPC can lower the algorithmic memory occupancy and execution time, which is consistent with Fig. 2 s analysis. In fact, the number of PWA regions of line-constrained EMPC is about an eighth of that of area-constrained EMPC when applied to an electric-drive system, saving large amounts of memory space.

In addition, EMPC could be utilized for overvoltage protection. For linearization purposes, the hexagon is utilized in place of the circlet to maintain the voltage within the limits. The formula for linear voltage constraints is given as follows:

$$G \cdot U_{dq} \le U_{\text{max}} \cdot E \tag{19}$$

where U_{max} is the maximum voltage allowed

$$U_{dq} = \begin{bmatrix} u_d(k) \\ u_q(k) \end{bmatrix}.$$

In conjunction with the current constraints, the total EMPC constraints are given as follows:

$$\begin{cases} i_d = F_{\text{lim}} \\ -I_{q\text{max}} \le i_q \le I_{q\text{max}} \\ G \cdot U_{dq} \le U_{\text{max}} \cdot E. \end{cases} \tag{20}$$

In addition, the length of the prediction horizon N_p needs to be tuned. According to Bolognani et al. [3], N_p has a minimum value, and under the condition of discretization, the state space is realized in discrete steps. In the method proposed in this study, the input U_{dq} is updated at time Kth and the current I_{dq} is updated at time $(k+1)$th; hence, it is sufficient for N_p to select 2 in this article.

C. Weight Factors

The Q matrix and R_u matrix in (8) require various weight factors due to the difficulty of uniting diverse control objectives. The weight factor tradeoff will have a substantial effect on the dynamic features of the system. However, there is currently no effective solution.

In this study, the line-constrained EMPC employs F_{lim} to restrict the d-axis current such that the controller has just one control objective, namely to track the q-axis current reference. The following is the Q matrix of the improved algorithm:

$$Q=\begin{bmatrix}0 & 0 & 0 & 0 & 0 & 0\\ 0 & \gamma_{iq} & 0 & 0 & -\gamma_{iq} & 0\\ 0 & 0 & 0 & 0 & 0 & 0\\ 0 & 0 & 0 & 0 & 0 & 0\\ 0 & -\gamma_{iq} & 0 & 0 & \gamma_{iq} & 0\\ 0 & 0 & 0 & 0 & 0 & 0\end{bmatrix} \tag{21}$$

where γ_{iq} is to keep the track of a q-axis current reference.

With no need to penalize the control action, the R_u shown in (8) is ignored.

Fig. 4 depicts the pole maps of the conventional and the proposed methods. In recent years, EMPCs weight factor tuning has not much improved; hence, the classic literature [3] is chosen for comparison. As seen in Fig. 4(a), the complex conjugate pole pair in the conventional method moves from the outside of the unit circle to the inside as γ_{iq} increases, and the real pole progressively approaches 1, which is identical to the analysis in [3]. However, Fig. 4(b) shows that the closed-loop poles of the improved algorithm do not move with the change of γ_{iq}. Therefore, the weight factors of line-constrained EMPC have no effect on the system's dynamic characters, thereby eliminating the need for weight factor tuning.

IV. Simulation Verification

Simulations under different conditions have examined the contrast between the line-constrained EMPC and the conventional methods. The proposed method employed a cascade controller where the speed loop used a PI controller and the current loop used a line-constrained EMPC controller (seen in Fig. 5). Table I displays the parameters. The conventional approaches, in contrast, employed the area-constrained EMPC technique. The traditional method I utilized the noncascaded EMPC controller presented in [3], and the traditional method II employed the EMPC current controller suggested in [27] with a PI controller in its speed loop. The model dimension of the tradition I is seven, whereas the proposed algorithm and the tradition II each have six dimensions. $N_p=5$ was selected in the comparison simulations

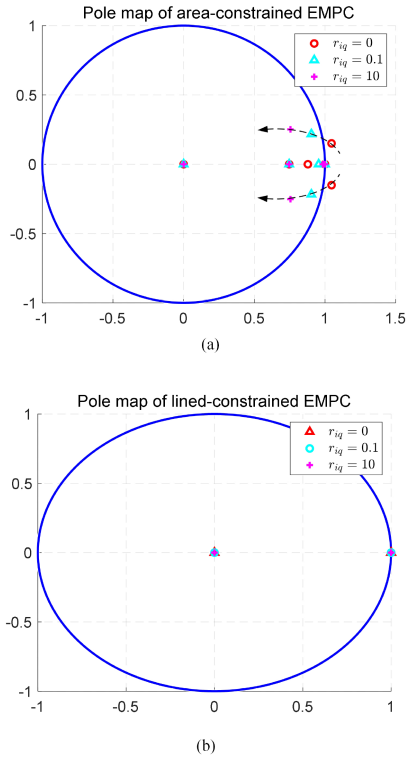

Fig. 4. Comparison of pole diagrams for (a) classical area-constrained EMPC and (b) proposed line-constrained EMPC.

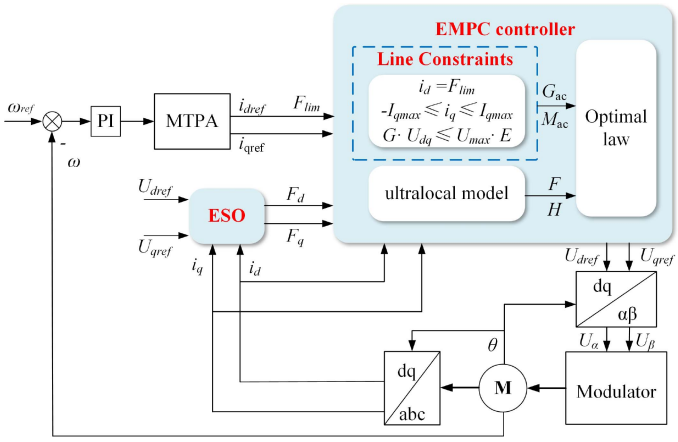

Fig. 5. Proposed diagram of MTPA implementation based on line-constrained EMPC controller.

TABLE I
IPMSM Parameters

Parameter	Value	Parameter	Value
R	0.43 Ω	ω_n	1500 r/ min
L_d	4.72 mH	I_n	14.8 A
L_q	12.4 mH	P_n	7.5 KW
p	4	T_n	47.7 N · m
λ_r	0.511 Wb	r_{iq}	1

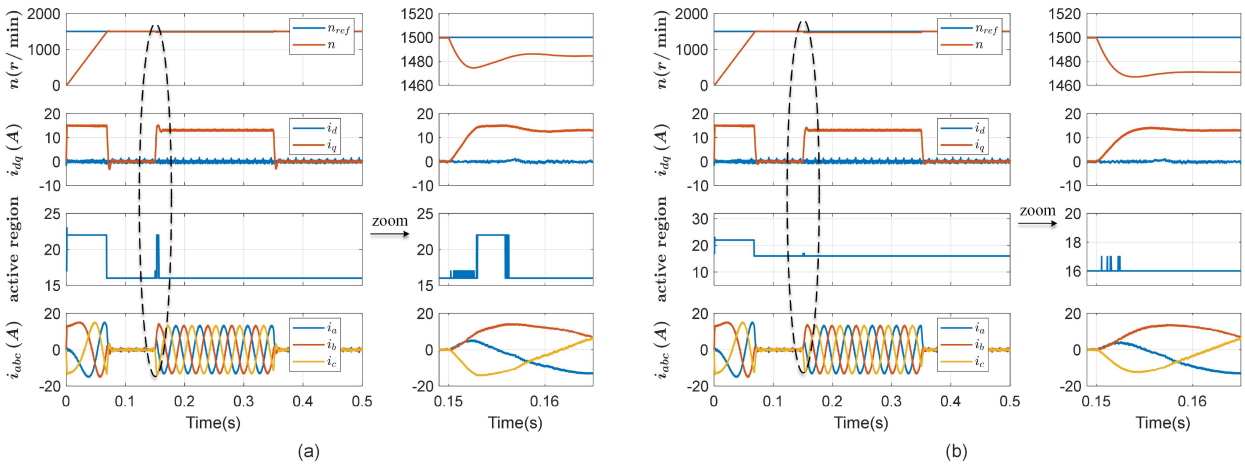

Fig. 6. Simulation of the traditional method I's dynamic response at (a) $r_{iq} = 0.01$ and (b) $r_{iq} = 0.5$.

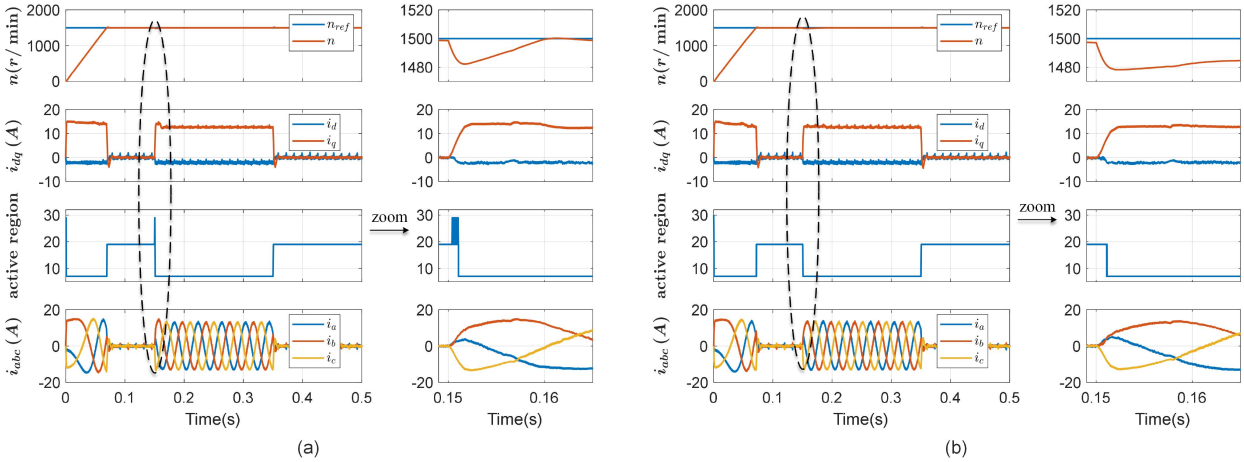

Fig. 7. Simulation of the traditional method II's dynamic response at (a) $r_{iq} = 0.01$ and (b) $r_{iq} = 0.5$.

to control variables. The simulation conditions comprise a step increase in motor speed from 0 r/min to the rated speed at 0 s and a step increase in motor torque from 0 N · m to 80% of the rated load at 0.15 s.

From the perspective of the explicit regions, it is observed in Fig. 6 that the step response of the traditional method I varies with respect to different r_{iq} values. Specifically, the active region is found to be between 15 and 40, despite the fact that the number of explicit regions exceeds 50.

Fig. 7 depicts the step response of the traditional method II. The number of explicit regions is 65 under $N_p = 5$, which is greater than in tradition I. It demonstrates that the explicit regions are not related to the model's size but rather to the type of constraints.

Fig. 8 depicts the step response of the proposed line-constrained EMPC. The active region is between 4 and 6, and the PWA regions' number is 7, which is about one-eighth of that of the traditional methods. Consequently, the line-constrained EMPC significantly reduces the memory occupancy.

From the perspective of weight factor calculation, it can be inferred from the graph that various values of r_{iq} affect the dynamic responsiveness of the system in the area-constrained EMPC. Second, from the perspective of weight factor calculation, reducing r_{iq} accelerates the current response but increases the current ripples. Moreover, when torque was applied, traditional method I suffered from steady-state errors in speed, indicating the poor performance of noncascaded EMPC under load. In comparison, the current characteristics of the improved algorithm eliminate the reliance on the weight factor computation and are capable of displaying a greater loading capacity. The results of the simulation are analyzed in the following text.

Due to the parameter tradeoff in the area-constrained EMPC system, alterations to the weight factor can significantly impact the response characteristics of the current loop. If the torque applied by the motor is not precisely controlled, the resulting speed of the motor may deviate from the desired steady-state speed.

The noncascaded area-constrained EMPC has a single controller for the inner and outer loops, and its cost function includes three control objectives, including the following of speed and current reference. In cases where the controller's slow torque response causes speed errors, the algorithm evaluates

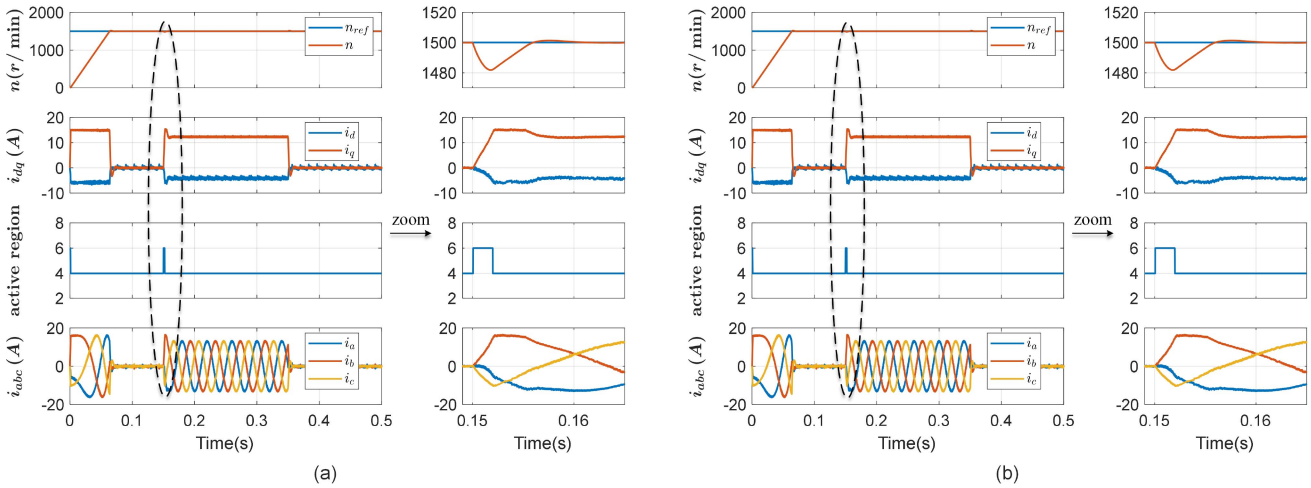

Fig. 8. Simulation of the proposed line-constrained EMPCs dynamic response at (a) $r_{iq} = 0.01$ and (b) $r_{iq} = 0.5$.

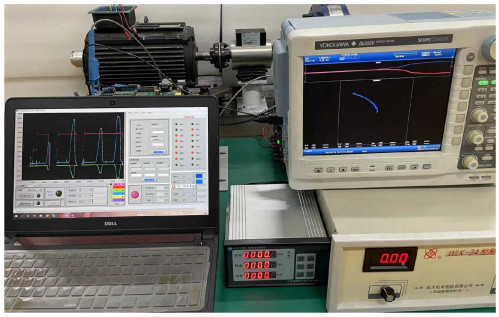

Fig. 9. Schematic diagram of the experimental platform.

TABLE II
PERFORMANCE OF EMPC WITH LINE CONSTRAINTS AND AREA CONSTRAINTS UNDER VARIOUS PARAMETERS

	N_p	2	3	4	5
Proposed line-constrained EMPC	m_I [kB]	4.0	4.4	4.8	5.1
	N_R	7	7	7	7
	t_E [us]	60	63	63.5	63.5
Traditional method I	m_I [kB]	19.0	41.8	44.13	60.19
	N_R	19	42	45	55
	t_E [us]	401.5	640	565	665
Traditional method II	m_I [kB]	16.68	35.17	38.68	42.8
	N_R	33	64	64	65
	t_E [us]	238	405	427	425.5

both control objectives to determine an optimal solution that balances both objectives. However, due to the absence of an error compensation mechanism in the EMPC, steady-state speed errors can occur.

The cascaded area-constrained EMPC technique utilizes a PI controller to regulate the speed loop. In cases where a speed error arises, the output of the PI controller is incremented to compensate for the error. Consequently, the cascaded area-constrained EMPC technique exhibits a delayed response to changes in torque.

In the cascaded line-constrained EMPC cost function, there is just one control objective, which is to follow the q-axis current reference. There will be no steady-state speed error since the controller does not need to balance the control goals and the output is the optimal solution following the q-axis current reference. Simulations demonstrate the benefits of line-constrained EMPC in terms of PWA regions, weight factor calculation, and load capacity.

V. EXPERIMENTAL RESULTS

The proposed line-constrained EMPC has been implemented on Infineon's XMC4500 platform, as shown in Fig. 9. The XMC4500 series belongs to the XMC4000 family of 32-bit ARM Cortex-M4-based microcontrollers for industrial applications. It has 120 MHz CPU frequency, 128 kB on-chip random access memory (RAM), and 1024 kB on-chip flash memory with 4 kB instruction cache. The EMPC data storage type was integer and the switching frequency was 10 kHz in this experiment. The 7.5 kW motor, whose characteristics are listed in Table I, was utilized. The load was applied to the motor through a magnetic powder brake. Throughout the experiment, the weight factor r_{iq} was assigned a value of 1 at unspecified locations.

A. Algorithm Comparison

The memory occupancy and execution efficiency of the proposed algorithm on the XMC4500 platform were validated and compared with the traditional method I and traditional method II. In Table II, the performance of the proposed method and the traditional methods in various prediction horizons is compared, where m_I indicates the RAM space occupied by EMPC data and code, N_R represents the number of explicit regions, and t_E represents the algorithm's execution time. The findings demonstrate that, initially, the dimension reduction can lower the algorithm's memory usage and execution time. However, the memory consumption and execution time of the line-constrained EMPC are much less than those of the

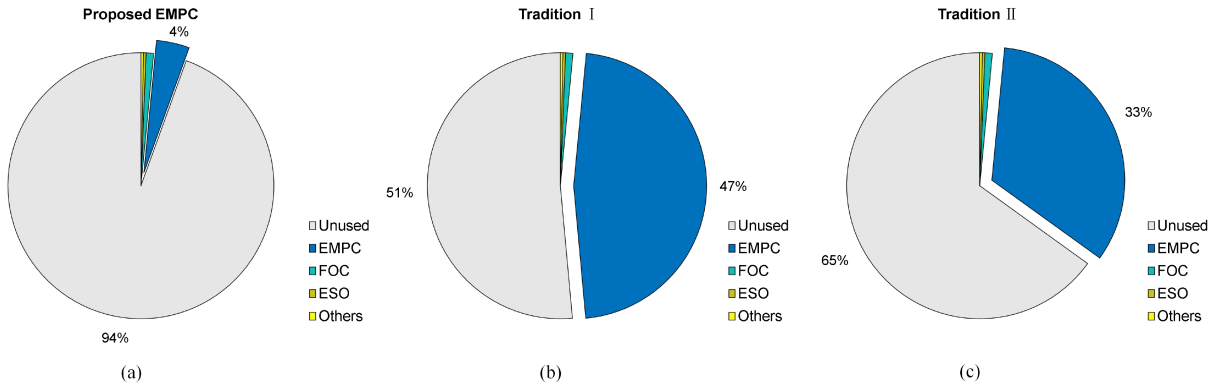

Fig. 10. Comparative analysis of RAM occupation when $N_p = 5$. (a) is the proposed line-constrained EMPC. (b) is the traditional method I. (c) is the traditional method II.

TABLE III
EMPC ALGORITHM COMPARISON

	Proposed EMPC	Tradition I	Tradition II
Constraints form	line	area	area
System dimension	6	7	6
Cascade or not	yes	no	yes
Minimum N_p length	2	4	2
Minimum memory occupancy	4 kB	44.13 kB	16.68 kB
Minimum number of regions	7	45	33
Minimum execution time	60 μs	565 μs	238 μs
Number of weigh factors	1	4	3
Weigh factor tweaking	no need	need	need

area-constrained EMPC for the same model dimensions. In addition, the explicit regions are not dependent on the size of the model but rather on the sort of constraints. The proposed method has a substantially fewer explicit regions than the conventional algorithm. Furthermore, the traditional methods cannot be implemented at a switching frequency of 10 kHz on this platform.

Fig. 10 compares the occupancy of RAM when $N_p = 5$. The findings indicate that the proposed approach only requires a modest amount of CPU memory, whereas the traditional methods take nearly half as much. Considering that 64 kB of XMC4500's RAM is on-chip data memory, the area-constrained EMPC consumes nearly all of the RAMs.

The comparison between the proposed method and the traditional methods is displayed in Table III. To evaluate the applicability to embedded devices, N_p of the three comparison algorithms was chosen as their minimum N_p length. It is concluded that line-constrained EMPC shows significant benefits in memory occupancy, execution time, and weight factor calculation. This enables EMPC to be applied to large-scale issues.

B. Response Characteristic

Figs. 11 and 12 show the step response of the proposed method under various torque and speed conditions. In Fig. 11, the motor speed was stepped from 600 to 1200 $\mathrm{r/min}$ with a load of 30%. And in Fig. 12, the motor speed was stepped

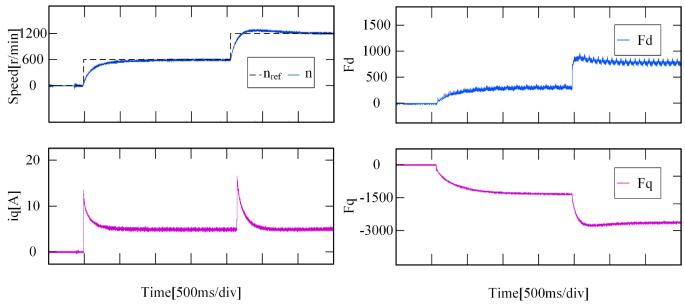

Fig. 11. Step response of the line-constrained EMPC under multispeed and 30% rate torque.

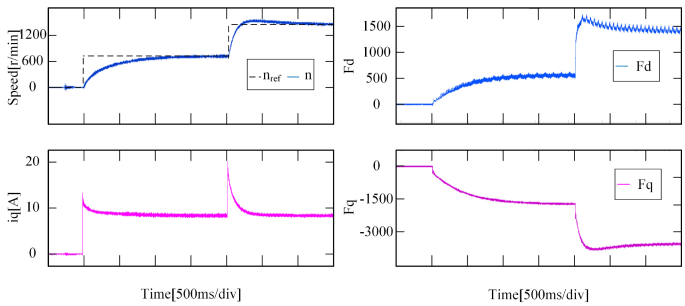

Fig. 12. Step response of the line-constrained EMPC under multispeed and 60% rate torque.

from 750 to 1500 $\mathrm{r/min}$ with a load of 60%. As shown in the figure, the motor's response speed is rapid when starting with a load. F_d is proportional to both speed and i_q, whereas F_q is only proportional to speed, which is consistent with the analysis presented before. The findings reveal that the line-constrained EMPC has good overall performance, and the viability of the scheme is proven.

To evaluate the steady-state properties of the proposed algorithm, comparative experiments of line-constrained EMPC with ESO and without ESO have been designed under 100% L and 150% L, respectively. The motor speed was 120 $\mathrm{r/min}$, and the load was 40%. Figs. 13 and 14 represent the experimental results. The experimental results indicate that the steady-state properties of the two modes are similar when the inductance parameters are

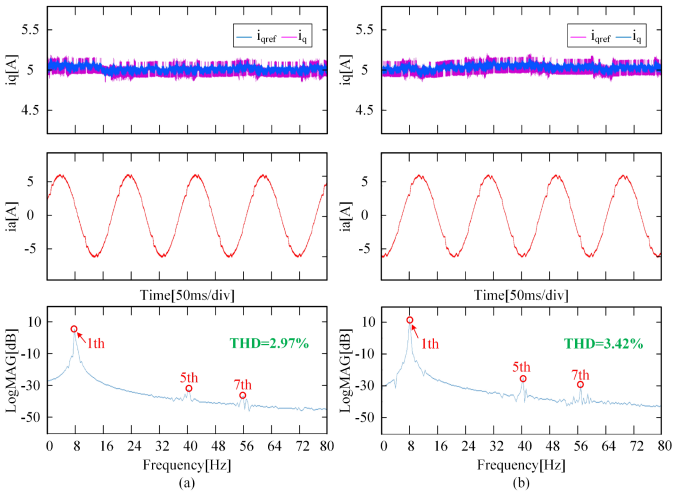

Fig. 13. Experimental results of the steady-state performance under 100% L at 120 r/min and 40% rate torque. (a) Proposed line-constrained EMPC with ESO. (b) Proposed line-constrained EMPC without ESO.

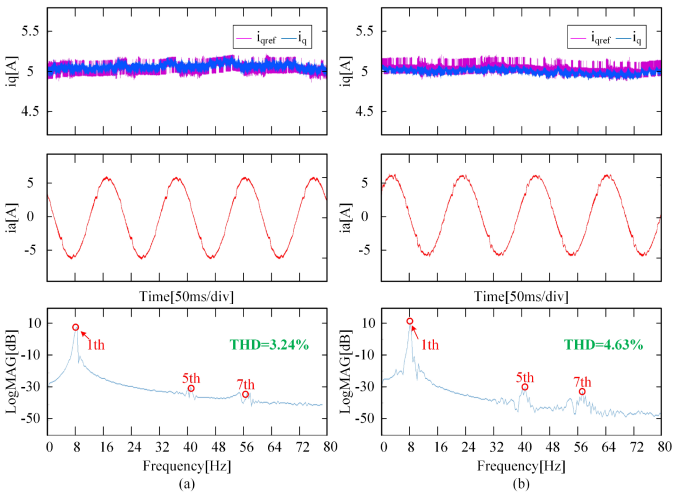

Fig. 14. Experimental results of the steady-state performance under 150% L at 120 r/min and 40% rate torque. (a) Proposed line-constrained EMPC with ESO. (b) Proposed line-constrained EMPC without ESO.

matched. Nevertheless, the total harmonic distortion (THD) of the line-constrained EMPC scheme with ESO drops by around 1.4% compared with the scheme without ESO under 150% L, and the noise of the q-axis current is also reduced. The experimental results demonstrate that the line-constrained EMPC with ESO has greater robustness and steady-state properties.

Fig. 15 depicts the step response of the dq-axis current. The response time of dq-axis current to command change is 5 ms, and there is no stability error. The results show that there is no discernible difference between the d-axis and q-axis current responses produced through constraint processing and cost function optimization, respectively. Fig. 16 is a detailed display of Fig. 15.

The performance of line-constrained EMPC in MTPA control is depicted in Fig. 17. Specifically, when the motor was operated at its rated speed, the load was increased to its rated value. In

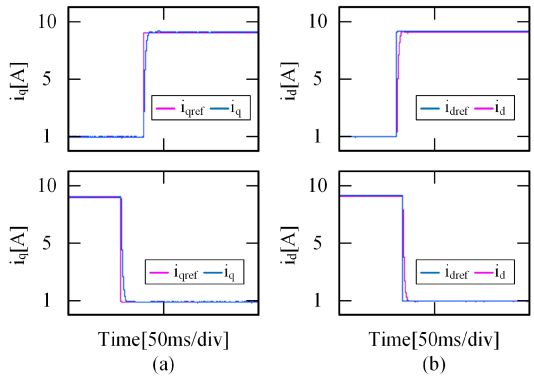

Fig. 15. Step response of the dq-axis current.

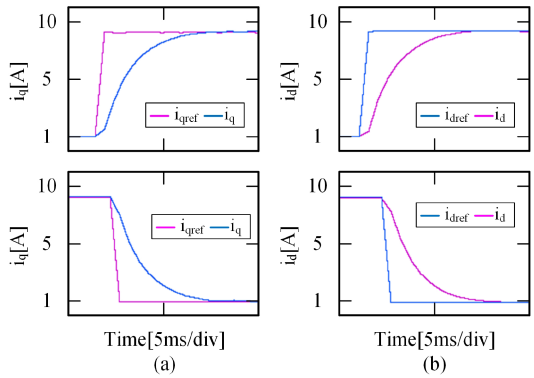

Fig. 16. Display of step response of the dq-axis current in detail.

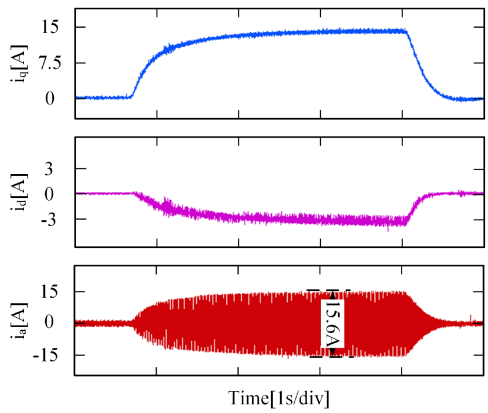

Fig. 17. Performance of MTPA control with line-constrainted EMPC under rate speed and rate torque.

particular, when the torque was 30 N · m, the experimentally determined dq-axis currents were −3.51 and 15.21 A, and their theoretical values are −3.30 and 14.82 A. The theoretical results are compatible with the actual ones. The experimental findings demonstrate that the line-constrained EMPC can effectively limit the d-axis current and has a high load capacity.

C. Active Region and Constraints

EMPC provides excellent constraint-handling capabilities. The active region selection of EMPC is linked to the active

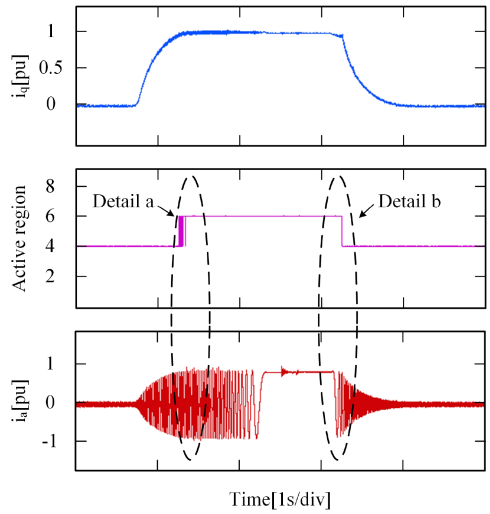

Fig. 18. Performance of linear EMPC under constraint (16), rate speed.

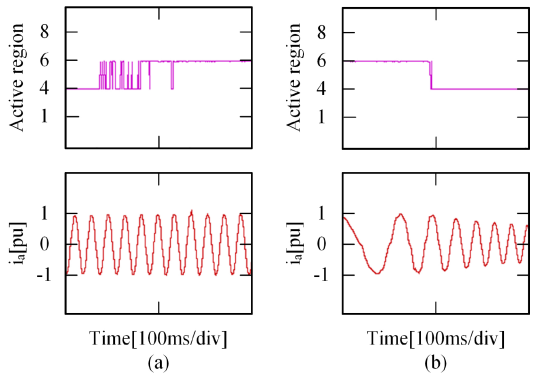

Fig. 19. Detail display diagram of (a) delta a and (b) delta b.

constraints based on the study in the section II. Fig. 18 depicts the action taken by EMPC controller when the constraint (16) was active. The experimental setup entailed running the motor at its rated speed and applying a load such that the load current exceeded the constraint limit (16). The active region changed when i_q reached $i_{q\max}$, preventing the current from increasing further. If torque increased further, the motor would stop. The active region reverted to its former state when i_q fell below $i_{q\max}$ and the controller regained its ability to modify the current. Fig. 19 depicts the detailed display of Fig. 18.

Fig. 20 shows the behavior of the EMPC controller when constraint (15) was activated, where $U_{\max}$ was set to 50 V. The motor speed was stepped to 300 $\mathrm{r/min}$ so that the voltage references exceeded the constraint limit (18). Likewise, the voltage was limited to $U_{\max}$ with the active region changed, and the speed could not reach the reference. To be specific, the experimentally values of U_d and U_q were -6.51 V and 52.21 V, respectively. In conclusion, the alteration of active constraints modifies the selection of active region, allowing the EMPC controller to limit state and input, which is consistent with the analysis in Section IV.

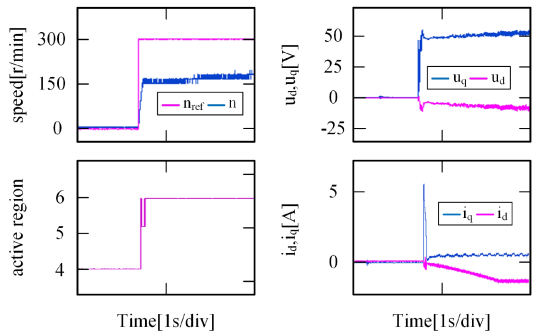

Fig. 20. Performance of linear EMPC under voltage constraint (18).

VI. Conclusion

This study's objective is to propose a line-constrained EMPC method for IPMSMs that reduces memory occupancy, enhances efficiency, and resolves the computation of weight factors. By constructing an ultralocal model of the motor, the system size is minimized. The addition of a new state variable converts the conventional EMPC area constraints into the line constraints expression. The main findings of the study are as follows.

1) Line-constrained EMPC improves efficiency by altering the constraints' expression form. It is demonstrated that the number of explicit regions of the proposed method is just 7, that its memory use is one-tenth that of the conventional algorithm and that its execution performance is ten times quicker.
2) The proposed method simplifies the cost function of the EMPC algorithm to contain just one parameter. The results indicate that a single weight factor has no effect on the operation of the controller, thus resolving the issue of calculating weight factors for EMPC.
3) The selection of the EMPC active region is related to the constraint triggering. The active region changes when the state variables surpass the limitations.
4) The controller with the proposed method has good performance and enables the EMPC constraint capability to be fully realized. The enhancement of execution efficiency facilitates the expansion of EMPCs application scope in the electric-drive industry.

There are still some problems that need to be further studied. First, how the active region impacts the system's dynamic performance requires a more detailed derivation. Second, whether the constraint processing capability of EMPC can be used to tackle more issues, such as deep weak magnetic fields, is a future study direction.

References

[1] J.-M. Mun, G.-J. Park, S. H. Seo, D.-W. Kim, Y.-J. Kim, and S.-Y. Jung, "Design characteristics of IPMSM with wide constant power speed range for EV traction," *IEEE Trans. Magn.*, vol. 53, no. 6, Jun. 2017, Art. no. 8105104.

[2] Z. Mynar, L. Vesely, and P. Vaclavek, "PMSM model predictive control with field-weakening implementation," *IEEE Trans. Ind. Electron.*, vol. 63, no. 8, pp. 5156–5166, Aug. 2016.

[3] S. Bolognani, Silverio Bolognani, L. Peretti, and M. Zigliotto, "Design and implementation of model predictive control for electrical motor drives," *IEEE Trans. Ind. Electron.*, vol. 56, no. 6, pp. 1925–1936, Jun. 2009.
[4] A. Mora, J. Orellana, J. Juliet, and R. Cárdenas, "Model predictive torque control for torque ripple compensation in variable-speed PMSMs," *IEEE Trans. Ind. Electron.*, vol. 63, no. 7, pp. 4584–4592, Jul. 2016.
[5] A. A. Ahmed, B. K. Koh, H. S. Park, K.-B. Lee, and Y. I. Lee, "Finite-control set model predictive control method for torque control of induction motors using a state tracking cost index," *IEEE Trans. Ind. Electron.*, vol. 64, no. 3, pp. 1916–1928, Mar. 2017.
[6] J. Rodriguez et al., "Latest advances of model predictive control in electrical drives–Part II: Applications and benchmarking with classical control methods," *IEEE Trans. Power Electron.*, vol. 37, no. 5, pp. 5047–5061, May 2022.
[7] F. Wang, L. He, and J. Rodriguez, "FPGA-based continuous control set model predictive current control for PMSM system using multistep error tracking technique," *IEEE Trans. Power Electron.*, vol. 35, no. 12, pp. 13455–13464, Dec. 2020.
[8] A. A. Ahmed, B. K. Koh, and Y. I. Lee, "A comparison of finite control set and continuous control set model predictive control schemes for speed control of induction motors," *IEEE Trans. Ind. Inform.*, vol. 14, no. 4, pp. 1334–1346, Apr. 2018.
[9] X. Luo, A. Shen, Q. Tang, J. Liu, and J. Xu, "Two-step continuous-control set model predictive current control strategy for SPMSM sensorless drives," *IEEE Trans. Energy Convers.*, vol. 36, no. 2, pp. 1110–1120, Jun. 2021.
[10] S. Rubino, R. Bojoi, S. A. Odhano, and P. Zanchetta, "Model predictive direct flux vector control of multi-three-phase induction motor drives," *IEEE Trans. Ind. Appl.*, vol. 54, no. 5, pp. 4394–4404, Sep./Oct. 2018.
[11] A. Bemporad, M. Morari, V. Dua, and E. N. Pistikopoulos, "The explicit solution of model predictive control via multiparametric quadratic programming," in *Proc. Amer. Control Conf.*, 2000, pp. 872–876.
[12] P. Cortes, J. Rodriguez, C. Silva, and A. Flores, "Delay compensation in model predictive current control of a three-phase inverter," *IEEE Trans. Ind. Electron.*, vol. 59, no. 2, pp. 1323–1325, Feb. 2012.
[13] G. Cimini, D. Bernardini, S. Levijoki, and A. Bemporad, "Embedded model predictive control with certified real-time optimization for synchronous motors," *IEEE Trans. Control Syst. Technol.*, vol. 29, no. 2, pp. 893–900, Mar. 2021.
[14] C. Wang, M. Yang, W. Zheng, J. Long, and D. Xu, "Vibration suppression with shaft torque limitation using explicit MPC-PI switching control in elastic drive systems," *IEEE Trans. Ind. Electron.*, vol. 62, no. 11, pp. 6855–6867, Nov. 2015.
[15] J. Bocker, B. Freudenberg, A. The, and S. Dieckerhoff, "Experimental comparison of model predictive control and cascaded control of the modular multilevel converter," *IEEE Trans. Power Electron.*, vol. 30, no. 1, pp. 422–430, Jan. 2015.
[16] L. He, F. Wang, J. Wang, and J. Rodriguez, "Zynq implemented Luenberger disturbance observer based predictive control scheme for PMSM drives," *IEEE Trans. Power Electron.*, vol. 35, no. 2, pp. 1770–1778, Feb. 2020.
[17] M. Chen, F. Wang, L. He, D. Ke, K. Zuo, and J. Rodriguez, "Predictive current control of permanent magnet synchronous motor based on an adaptive internal model observer," in *Proc. IEEE 9th Int. Power Electron. Motion Control Conf.*, 2020, pp. 2567–2571.
[18] Y. Zhang, J. Jin, and L. Huang, "Model-free predictive current control of PMSM drives based on extended state observer using ultralocal model," *IEEE Trans. Ind. Electron.*, vol. 68, no. 2, pp. 993–1003, Feb. 2021.
[19] J. Min, S. Fuchs, and J. Biela, "When FPGAs meet regionless explicit MPC: An implementation of long-horizon linear MPC for power electronic systems," in *Proc. 46th Annu. Conf. IEEE Ind. Electron. Soc.*, 2020, pp. 3085–3092.
[20] J. Rodriguez et al., "Latest advances of model predictive control in electrical drives–Part I: Basic concepts and advanced strategies," *IEEE Trans. Power Electron.*, vol. 37, no. 4, pp. 3927–3942, Apr. 2022.
[21] L. M. A. Caseiro, A. M. S. Mendes, and S. M. A. Cruz, "Dynamically weighted optimal switching vector model predictive control of power converters," *IEEE Trans. Ind. Electron.*, vol. 66, no. 2, pp. 1235–1245, Feb. 2019.
[22] O. Machado, P. Martín, F. J. Rodríguez, and E. J. Bueno, "A neural network-based dynamic cost function for the implementation of a predictive current controller," *IEEE Trans. Ind. Inform.*, vol. 13, no. 6, pp. 2946–2955, Dec. 2017.
[23] M. Novak, H. Xie, T. Dragicevic, F. Wang, J. Rodriguez, and F. Blaabjerg, "Optimal cost function parameter design in predictive torque control (PTC) using artificial neural networks (ANN)," *IEEE Trans. Ind. Electron.*, vol. 68, no. 8, pp. 7309–7319, Aug. 2021.
[24] M. Kvasnica, P. Grieder, M. Baotic, and F. J. Christophersen, "Multi-parametric toolbox," Lecture Notes in Computer Science, 2006. [Online]. Available: http://people.ee.ethz.ch/mpt/2/
[25] A. Bemporad, M. Morari, V. Dua, and E. N. Pistikopoulos, "The explicit linear quadratic regulator for constrained systems," *Automatica*, vol. 38, no. 1, pp. 3–20, 2002.
[26] J. Liu, C. Gong, Z. Han, and H. Yu, "IPMSM model predictive control in flux-weakening operation using an improved algorithm," *IEEE Trans. Ind. Electron.*, vol. 65, no. 12, pp. 9378–9387, Dec. 2018.
[27] C. Jia, X. Wang, Y. Liang, and K. Zhou, "Robust current controller for IPMSM drives based on explicit model predictive control with online disturbance observer," *IEEE Access*, vol. 7, pp. 45898–45910, 2019.

Han Wang received the B.S. degree in electrical engineering from Fuzhou University, Fuzhou, China, in 2017, and the M.S. degree in electrical engineering in 2020 from the Harbin Institute of Technology, Harbin, China, where he is currently working toward the Ph.D. degree with the School of Electrical Engineering.

His current research interests include motor drive, model predictive control, and adaptive control.

Jianyong Su (Member, IEEE) was born in China in 1979. He received the B.S., M.S., and Ph.D. degrees in electrical engineering from the Harbin Institute of Technology (HIT), Harbin, China, in 2002, 2004, and 2009, respectively.

He is currently an Associate Professor with the School of Electrical Engineering and Automation, HIT. From June 2015 to May 2016, he was a Visiting Scholar with North Carolina State University, Raleigh, USA. His current research interests include multiphase PMSM, low-voltage IM, model predictive control, and sensorless control.

Guijie Yang (Member, IEEE) was born in China in 1965. He received the Ph.D. degree in electrical engineering from the Harbin Institute of Technology (HIT), Harbin, China, in 2005.

Since 1992, he has been an Assistant Researcher with the Research Center of Inertial Navigation Equipment, HIT. From 1998 to 2004, he was an Associate Professor with HIT, where since 2004, he has been a Professor with the School of Electrical Engineering and Automation. His current research interests include high-power PMSG drives, integrated digital control for motors, and motor-drive IP core-based FPGAs.